

A Fully Natural Gradient Scheme for Improving Inference of the Heterogeneous Multi-Output Gaussian Process Model

Juan-José Giraldo and Mauricio A. Álvarez

Department of Computer Science, University of Sheffield

Abstract

A recent novel extension of multi-output Gaussian processes handles heterogeneous outputs assuming that each output has its own likelihood function. It uses a vector-valued Gaussian process prior to jointly model all likelihoods' parameters as latent functions drawn from a Gaussian process with a linear model of coregionalisation covariance. By means of an inducing points framework, the model is able to obtain tractable variational bounds amenable to stochastic variational inference. Nonetheless, the strong conditioning between the variational parameters and the hyper-parameters burdens the adaptive gradient optimisation methods used in the original approach. To overcome this issue we borrow ideas from variational optimisation introducing an exploratory distribution over the hyper-parameters, allowing inference together with the variational parameters through a fully natural gradient optimisation scheme. We show that our optimisation scheme can achieve better local optima solution with higher test performance rates than adaptive gradient methods or an hybrid strategy that partially use natural gradients in cooperation with the Adam method. We compare the performance of the different methods over toy and real databases.

1 Introduction

A Multi-Output Gaussian Process (MOGP) model generalises the Gaussian Process (GP) model by exploiting correlations not only in the input space, but also in the output space (Álvarez et al., 2012). The major research about MOGP models has focused on finding proper definitions of a cross-covariance function between the multiple outputs (Journal and Huijbregts, 1978; Higdon, 2002). Nevertheless few works have been concerned about targeting the issue that those outputs not necessarily follow the same statistical data type. To address that regard, a recent approach known as the Heterogeneous Multi-Output Gaussian Process (HetMOGP) model extends the MOGP application (Álvarez and Lawrence, 2009) to any arbitrary combination of D likelihood distributions over the output observations (Moreno-Muñoz et al., 2018). It can be seen as a generalisation of a Chained GP (Saul et al., 2016) for multiple correlated output functions of an heterogeneous nature. The HetMOGP's scalability bases on the schemes: variational inducing kernels for efficient MOGPs (Álvarez et al., 2010) and variational inducing variables for single-output GPs (Hensman et al., 2013). These schemes rely on the idea of augmenting the GP prior probability space, through the inclusion of a so-called set of inducing points that change the full GP covariance by a low-rank approximation (Quiñonero-Candela and Rasmussen, 2005; Snelson and Ghahramani, 2006). Such inducing points help reducing significantly the MOGP's computational costs from $\mathcal{O}(D^2N^2)$ to $\mathcal{O}(DNM^2)$ and storage from $\mathcal{O}(D^3N^3)$ to $\mathcal{O}(DNM)$, where N , D and $M \ll N$ represent the number of data observations, outputs and inducing points, respectively (Rasmussen, 2006; Álvarez and Lawrence, 2009).

The adequate performance of a variational GP model depends on a proper optimisation process able to find rich local optima solutions for maximising a bound to the marginal likelihood. The variational GP models generally suffer from strong conditioning between the variational posterior distribution, the multiple hyper-parameters of the GP prior and the inducing points (van der Wilk, 2018). In particular, the HetMOGP model is built upon a linear combinations of Q latent functions, where each latent function demands a treatment based on the inducing variables framework. On this model then, such strong conditionings are enhanced even more due to the dependence of inducing points per underlying latent function, and the presence of additional linear combination coefficients. Since the model is extremely sensitive to any small change on any of those variables, stochastic gradient updates in combination with adaptive gradient methods (AGMs, e.g. Adam) tend to drive the optimisation to poor local minima. With the purpose to overcome the optimisation problems present in variational GP models, there has recently been a growing interest in alternative optimisation schemes that adopt the natural gradient (NG) direction (Amari, 1998). For instance, in (Hensman et al., 2013) the authors derived a mathematical analysis that suggested we can make

better progress when optimising a variational GP along the natural gradient direction, but without providing any experimental results of its performance. The authors in (Khan et al., 2015) propose to linearise the non-conjugate terms of the model for admitting closed-form updates which are equivalent to optimising in the natural gradient direction. The work in (Khan and Lin, 2017) shows how to convert inference in non-conjugate models as it is done in the conjugate ones, by way of expressing the posterior distribution in the mean-parameter space. Furthermore, it shows that by means of exploiting the mirror descent algorithm one can arrive to natural gradient updates for tuning the variational posterior distribution. Those works coincide in improvements of training and testing performance, and also fast convergence rates. Nonetheless, they only show results in a full GP model where the kernel hyper-parameters are fixed using a grid search. On the other hand, the work in (Salimbeni et al., 2018) does show a broad experimental analysis of the natural gradient method for sparse GPs. The authors conclude that the natural gradient is not prone to suffer from ill-conditioning issues in comparison to the AGMs. Also the natural gradient has been used to ease optimisation of the variational posterior over the latent functions of a deep GP model (Salimbeni et al., 2019). However, in those two latter cases the natural gradient method only applies for the latent functions’ posterior parameters, while an Adam method performs a cooperative optimisation for dealing with the hyper-parameters and inducing points. The authors in (Salimbeni et al., 2018) call this strategy an hybrid between natural gradient and Adam, and termed it NG+Adam.

In this paper, we propose a fully natural gradient scheme for tuning the hyper-parameters, inducing points and variational posterior parameters all together. To this end, we borrow ideas from different variational optimisation (VO) strategies like (Staines and Barber, 2013; Khan et al., 2017a) and (Khan et al., 2018), by introducing an exploratory distribution over the hyper-parameters and inducing points. Such VO strategies have shown to be successful exploratory-learning tools able to avoid poor local optima solutions; they have been broadly studied in the context of reinforcement and Bayesian deep learning, but not much in the context of GPs. To the best of our knowledge the NG method has not been performed over any MOGP model before. Therefore, our main contribution in this work consist on showing for the first time how a NG method used in a full scheme over the HetMOGP’s parameters and kernel hyper-parameters alleviates the strong conditioning problems. This, by achieving better local optima solutions with higher test performance rates than Adam and stochastic gradient descent. Furthermore, we explore for the first time in a MOGP model the behaviour of the hybrid strategy NG+Adam, and provide comparative results to our proposed scheme.

2 Variational Optimisation: an Exploratory Mechanism for Optimisation

This section introduces the variational optimisation method as an exploratory mechanism for minimising an objective function (Staines and Barber, 2013). It also shows how variational inference can be seen as a particular case of variational optimisation.

2.1 Variational Optimisation

The goal in optimisation is to find a proper set of parameters that minimise a possibly non-convex function $g(\theta)$ by solving,

$$\theta^* = \arg \min_{\theta} g(\theta), \quad (1)$$

where θ^* represents the set of parameters that minimise the function. The classical way to deal with the above optimisation problem involves deriving w.r.t θ and solving in a closed-form, or through a gradient descent method. Usually, gradient methods tend to converge to the closest local minima from the starting point without exploring much the space of solutions (Chong and Zak, 2013). Alternatively the variational optimisation method proposes to solve the same problem, but introducing exploration in the parameter space of an auxiliary distribution $q(\theta|\eta)$ by bounding the function $g(\theta)$ as follows:

$$\min_{\theta} g(\theta) \leq \mathbb{E}_{q(\theta|\psi)}[g(\theta)] := \tilde{\mathcal{L}}(\psi), \quad (2)$$

where ψ represents a set of variables that parametrise the distribution $q(\theta|\psi)$, and $\tilde{\mathcal{L}}(\psi)$ is an upper bound to the function $g(\theta)$. Therefore the main goal is to minimize the above equation w.r.t the new set ψ . For instance, if we start an optimisation process to solve the last problem, and set an exploratory Gaussian distribution $q(\theta|\mu, \Sigma)$, where the set ψ is composed by the mean μ and covariance Σ . Then, at the beginning of such optimisation process

our covariance initialisation should be $\Sigma \neq \mathbf{0}$, meaning that the space of solutions can be explored around the initial mean $\boldsymbol{\mu}$ (Wierstra et al., 2014). After the optimisation time elapses, the mean $\boldsymbol{\mu}$ will be approaching to a local minima $\boldsymbol{\theta}^*$ that best reduces the expectation in Eq. (2), while the covariance Σ will be collapsing ($\Sigma \rightarrow \mathbf{0}$). Thereby the exploratory distribution will become a Dirac’s delta $q(\boldsymbol{\theta}) = \delta(\boldsymbol{\theta} - \boldsymbol{\mu})$, where $\boldsymbol{\mu} = \boldsymbol{\theta}^*$ (Hensman et al., 2015b). The covariance’s collapsing behaviour is an indicator of how the exploration reduces while the objective is converging to a local minimum. In order to gain wider exploration, we can avoid Σ to collapse by imposing a regularization term to the latter bound:

$$\tilde{\mathcal{L}}(\boldsymbol{\psi}) = \mathbb{E}_{q(\boldsymbol{\theta}|\boldsymbol{\psi})}[g(\boldsymbol{\theta})] + \mathbb{D}_{KL}(q(\boldsymbol{\theta}|\boldsymbol{\psi})||p(\boldsymbol{\theta})), \quad (3)$$

where $\mathbb{D}_{KL}(\cdot||\cdot)$ is a Kullback-Leibler (KL) divergence which forces the auxiliary distribution $q(\boldsymbol{\theta}|\boldsymbol{\psi})$ to trade-off between minimising the expectation of the function $g(\boldsymbol{\theta})$ and not going far away from an imposed $p(\boldsymbol{\theta})$ penalization distribution (Khan et al., 2017b).

2.2 Variational Inference: VO for the Negative Log Likelihood

A common way to build a probabilistic model for a set of observations $\mathbf{X} = \{\mathbf{x}_n\}_{n=1}^N \in \mathbb{R}^{N \times P}$ is to assume that each observation is drawn from the same probability distribution $p(\mathbf{X}|\boldsymbol{\theta})$. Parameters $\boldsymbol{\theta}$ of such model are found by minimising the negative log likelihood (NLL) function $-\log p(\mathbf{X}|\boldsymbol{\theta})$ (Murphy, 2013). If we follow the VO perspective in Eq. (3) assuming that the function we are interested in optimising is actually the NLL, $g(\boldsymbol{\theta}) = -\log p(\mathbf{X}|\boldsymbol{\theta})$, we can rewrite the bound as:

$$\tilde{\mathcal{L}}(\boldsymbol{\psi}) = -\mathbb{E}_{q(\boldsymbol{\theta}|\boldsymbol{\psi})} \left[\log \frac{p(\mathbf{X}|\boldsymbol{\theta})p(\boldsymbol{\theta})}{q(\boldsymbol{\theta}|\boldsymbol{\psi})} \right], \quad (4)$$

and notice that $-\tilde{\mathcal{L}}(\boldsymbol{\psi})$ is an evidence lower bound (ELBO) derived in variational inference (VI) with the purpose of approximating the true posterior $p(\boldsymbol{\theta}|\mathbf{X})$ by means of a free parameterised variational distribution $q(\boldsymbol{\theta}|\boldsymbol{\psi})$ (Blei et al., 2017). Likewise, the penalization distribution $p(\boldsymbol{\theta})$ is basically the prior knowledge over $\boldsymbol{\theta}$, and the bound in Eq. (2) can be seen as a particular case of (4) where $p(\boldsymbol{\theta}) = q(\boldsymbol{\theta})$. From a Bayesian perspective we are not only interested in the main positioning of the $q(\boldsymbol{\theta})$ ’s mean over $\boldsymbol{\theta}^*$, but also in the uncertainty codified in its (co)variance for making future predictions. On the other hand, since the main goal in VO is to optimise the function $g(\boldsymbol{\theta})$, for this particular case being the NLL, we can make use of only the posterior mean $\mathbb{E}_{q(\boldsymbol{\theta}|\boldsymbol{\psi})}[\boldsymbol{\theta}]$ as a feasible solution for $\boldsymbol{\theta}^*$ without taking into account the posterior’s uncertainty, also known as the maximum a posteriori solution (Bishop, 2006).

3 Exploiting The Mirror Descent Algorithm

The purpose of this section is to show how the mirror descent algorithm can induce a natural gradient algorithm to solve a VO problem. Also, we introduce the Variational Adaptive-Newton (VAN) method and the concept of *natural-momentum*.

3.1 From the Mirror Descent to the Natural-Gradient

Let us assume an optimisation problem like the one in Eq. (2), where the goal consists in finding an optimal distribution $q_{\boldsymbol{\theta}} := q(\boldsymbol{\theta}|\boldsymbol{\eta})$ that best minimises the objective bound. To this end, we assume an exponential-family distribution $q_{\boldsymbol{\theta}}$, so that a mirror descent algorithm can be formulated on its mean-parameter space.¹ Then the algorithm bases on solving the following iterative sub-problems:

$$\boldsymbol{\eta}_{t+1} = \arg \min_{\boldsymbol{\eta}} \langle \boldsymbol{\eta}, \hat{\nabla}_{\boldsymbol{\eta}} \tilde{\mathcal{L}}_t \rangle + \frac{1}{\alpha_t} \mathbb{D}_{KL}(q_{\boldsymbol{\theta}}||q_{\boldsymbol{\theta}_t}), \quad (5)$$

where $\boldsymbol{\eta}$ is the set of $q_{\boldsymbol{\theta}}$ ’s mean-parameters, $\tilde{\mathcal{L}}$ is a VO bound of a function $g(\boldsymbol{\theta})$, $\hat{\nabla}_{\boldsymbol{\eta}} \tilde{\mathcal{L}}_t := \hat{\nabla}_{\boldsymbol{\eta}} \tilde{\mathcal{L}}(\boldsymbol{\eta}_t)$ denotes a stochastic gradient, $q_{\boldsymbol{\theta}_t} := q(\boldsymbol{\theta}|\boldsymbol{\eta}_t)$ and α_t is a positive step-size parameter (Khan and Lin, 2017). The intention of the above formulation is to exploit the parametrised distribution’s structure by controlling its divergence w.r.t its older state $q_{\boldsymbol{\theta}_t}$. Thereby, solving the above problem in the mean-parameter space induces a natural gradient descent

¹An exponential-family distribution $q_{\boldsymbol{\theta}}$ has an associated set of mean-parameters $\boldsymbol{\eta} = \mathbb{E}[\boldsymbol{\phi}(\boldsymbol{\theta})]$, where $\boldsymbol{\phi}$ represents the vector of sufficient statistics.

update in the natural-parameter space of the distribution. The authors in (Raskutti and Mukherjee, 2015) provide a formal proof of such equivalence where:

$$\begin{aligned}\boldsymbol{\lambda}_{t+1} &= \boldsymbol{\lambda}_t - \alpha_t \hat{\nabla}_{\boldsymbol{\eta}} \tilde{\mathcal{L}}_t \\ &= \boldsymbol{\lambda}_t - \alpha_t \mathbf{F}^{-1} \hat{\nabla}_{\boldsymbol{\lambda}} \tilde{\mathcal{L}}_t,\end{aligned}\tag{6}$$

here $\boldsymbol{\lambda}$ represents the natural (or canonical) parameters of the distribution $q_{\boldsymbol{\theta}}$, \mathbf{F} is the Fisher information matrix associated to the random variable $\boldsymbol{\theta}$, and $\hat{\nabla}_{\boldsymbol{\lambda}} \tilde{\mathcal{L}}_t := \hat{\nabla}_{\boldsymbol{\lambda}} \tilde{\mathcal{L}}(\boldsymbol{\lambda}_t)$ denotes a stochastic gradient w.r.t those natural parameters. The formulation in Eq. (5) is advantageous since it is easier to compute derivatives w.r.t $\boldsymbol{\eta}$ than computing the inverse Fisher information matrix \mathbf{F}^{-1} .

3.2 Variational Adaptive-Newton Method

The VAN method aims to solve the problem in Eq. (5) using a Gaussian distribution $q_{\boldsymbol{\theta}} := q(\boldsymbol{\theta}|\boldsymbol{\mu}, \boldsymbol{\Sigma})$ as the exploratory mechanism for optimisation (Khan et al., 2017a). This implies that if $\boldsymbol{\mu}$ and $\boldsymbol{\Sigma}$ represent the mean and covariance respectively, then $q_{\boldsymbol{\theta}}$'s mean-parameters are $\boldsymbol{\eta} = \{\boldsymbol{\mu}, \boldsymbol{\Sigma} + \boldsymbol{\mu}\boldsymbol{\mu}^\top\}$, and also its analogous natural-parameters are $\boldsymbol{\lambda} = \{\boldsymbol{\Sigma}^{-1}\boldsymbol{\mu}, -\frac{1}{2}\boldsymbol{\Sigma}^{-1}\}$. When plugging these parametrisations and solving for the mirror descent algorithm in Eq. (5), we end up with the following updates:

$$\boldsymbol{\Sigma}_{t+1}^{-1} = \boldsymbol{\Sigma}_t^{-1} + 2\alpha_t \hat{\nabla}_{\boldsymbol{\Sigma}} \tilde{\mathcal{L}}_t\tag{7}$$

$$\boldsymbol{\mu}_{t+1} = \boldsymbol{\mu}_t - \alpha_t \boldsymbol{\Sigma}_{t+1} \hat{\nabla}_{\boldsymbol{\mu}} \tilde{\mathcal{L}}_t,\tag{8}$$

where $\boldsymbol{\mu}_t$ and $\boldsymbol{\Sigma}_t$ are the mean and covariance parameters at the instant t respectively; the stochastic gradients are $\hat{\nabla}_{\boldsymbol{\mu}} \tilde{\mathcal{L}}_t := \hat{\nabla}_{\boldsymbol{\mu}} \tilde{\mathcal{L}}(\boldsymbol{\mu}_t, \boldsymbol{\Sigma}_t)$ and $\hat{\nabla}_{\boldsymbol{\Sigma}} \tilde{\mathcal{L}}_t := \hat{\nabla}_{\boldsymbol{\Sigma}} \tilde{\mathcal{L}}(\boldsymbol{\mu}_t, \boldsymbol{\Sigma}_t)$. These latter updates represent a natural gradient descent algorithm for exploring the space of solutions of the variable $\boldsymbol{\theta}$ through a Gaussian distribution (Khan and Lin, 2017).

3.3 Natural-Momentum Method

The natural gradient method takes advantage of the inverse Fisher information matrix for improving optimisation paths (Amari, 1998; Khan and Lin, 2017). The mirror descent algorithm shown before makes use of the Kullback-Leibler divergence for inducing the Fisher information matrix, thereby exploiting the structure of the exploratory distribution. In the interest of solving the same bound $\tilde{\mathcal{L}}$, it is still possible to keep exploiting the structure of that distribution $q_{\boldsymbol{\theta}}$ by including an additional KL divergence term as follows:

$$\boldsymbol{\eta}_{t+1} = \arg \min_{\boldsymbol{\eta}} \langle \boldsymbol{\eta}, \hat{\nabla}_{\boldsymbol{\eta}} \tilde{\mathcal{L}}_t \rangle + \frac{1}{\tilde{\alpha}_t} \mathbb{D}_{KL}(q_{\boldsymbol{\theta}} || q_{\boldsymbol{\theta}_t}) - \frac{\tilde{\gamma}_t}{\tilde{\alpha}_t} \mathbb{D}_{KL}(q_{\boldsymbol{\theta}} || q_{\boldsymbol{\theta}_{t-1}}),\tag{9}$$

where $q_{\boldsymbol{\theta}_{t-1}} := q(\boldsymbol{\theta}|\boldsymbol{\mu}_{t-1}, \boldsymbol{\Sigma}_{t-1})$ represents the exploratory distributions $q_{\boldsymbol{\theta}}$ with the parameters obtained at time $t-1$. Such additional KL term, called as a *natural-momentum* in (Khan et al., 2018), provides extra memory information to the mirror descent algorithm for potentially improving its convergence rate. This momentum can be controlled by the relation between the positive step-sizes $\tilde{\alpha}_t$ and $\tilde{\gamma}_t$. The update equations for the above problem are as follows:

$$\begin{aligned}\boldsymbol{\Sigma}_{t+1}^{-1} &= \boldsymbol{\Sigma}_t^{-1} + 2\alpha_t \hat{\nabla}_{\boldsymbol{\Sigma}} \tilde{\mathcal{L}}_t \\ \boldsymbol{\mu}_{t+1} &= \boldsymbol{\mu}_t - \alpha_t \boldsymbol{\Sigma}_{t+1} \hat{\nabla}_{\boldsymbol{\mu}} \tilde{\mathcal{L}}_t + \gamma_t \boldsymbol{\Sigma}_{t+1} \boldsymbol{\Sigma}_t^{-1} (\boldsymbol{\mu}_t - \boldsymbol{\mu}_{t-1}),\end{aligned}$$

where $\alpha_t = \tilde{\alpha}_t / (1 - \tilde{\gamma}_t)$ and $\gamma_t = \tilde{\gamma}_t / (1 - \tilde{\gamma}_t)$ are positive step-size parameters (Khan et al., 2018). Notice that here the parameter α_t is not the same of Eq. (5) unless we remove the momentum term by making $\tilde{\gamma}_t = 0$.

4 Heterogeneous Multi-Output Gaussian Process Model

This section explains the construction of the HetMOGP model. Also, how the inducing points framework allows the model to obtain tractable variational bounds amenable to stochastic variational inference.

4.1 The Likelihood Function

The HetMOGP model is an extension of the Multi-Output GP that allows different sorts of likelihoods as per the statistical data type each output demands (Moreno-Muñoz et al., 2018). For instance, if we have two outputs problem, where one output is binary $y_1 \in \{0, 1\}$ while the other is a real value $y_2 \in \mathbb{R}$, we can assume our likelihood as the

product of a Bernoulli and Gaussian distribution for each output respectively. In general the HetMOGP likelihood for D outputs can be written as:

$$p(\mathbf{y}|\mathbf{f}) = \prod_{n=1}^N \prod_{d=1}^D p(y_{d,n}|\mathbf{f}_{d,n}),$$

where $\mathbf{f}_{d,n} = [f_{d,1,n}, \dots, f_{d,J_d,n}]^\top$ and each $f_{d,j,n}$ is considered a latent parameter function (LPF) that comes from a linear combination of latent random processes as follows:

$$f_{d,j,n} = \sum_{q=1}^Q \sum_{i=1}^{R_q} a_{d,j,q}^i u_q^i(\mathbf{x}_n), \quad (10)$$

where $u_q^i(\mathbf{x})$ are samples from Gaussian Processes $u_q(\cdot) \sim \mathcal{GP}(0, k_q(\cdot, \cdot))$ taken independently and identically distributed (IID) and each linear combination coefficient $a_{d,j,q}^i \in \mathbb{R}$. Notice that each vector-valued function $\mathbf{f}_{d,n} \in \mathbb{R}^{J_d \times 1}$, where each J_d accounts for the number of latent functions necessary to parameterise each heterogeneous likelihood. So the total number of LPFs for the model becomes $J = \sum_{d=1}^D J_d$. Likewise, the number of linear combination coefficients per latent function $u_q(\cdot)$ becomes $J \times R_q$. Such number of coefficients can be grouped in a matrix $\mathbf{W}_q \in \mathbb{R}^{J \times R_q}$ with entries $\{a_{d,j,q}^i\}_{d=1, j=1, i=1}^{D, J_d, R_q}$. For the sake of future explanations let us assume that $R_q = 1$ and cluster all matrices \mathbf{W}_q in a specific vector of linear combination coefficients $\mathbf{w} = [\text{vec}(\mathbf{W}_1)^\top, \dots, \text{vec}(\mathbf{W}_Q)^\top]^\top \in \mathbb{R}^{QJ \times 1}$.

4.2 The Inducing Points Method

The GP models demand a high computational complexity for their inference processes. A common approach to induce sparsity for reducing such complexity is to augment the GP prior with a set of *inducing variables*. For the specific case of the HetMOGP model, those *inducing variables* are $\mathbf{u} = [\mathbf{u}_1^\top, \dots, \mathbf{u}_Q^\top]^\top \in \mathbb{R}^{QM \times 1}$ that represent additional function evaluations of some unknown inducing points $\mathbf{Z} = [\mathbf{Z}_1^\top, \dots, \mathbf{Z}_Q^\top]^\top \in \mathbb{R}^{QM \times P}$ respectively (Snelson and Ghahramani, 2006; Titsias, 2009). We can write the augmented GP prior as follows,

$$p(\mathbf{f}|\mathbf{u})p(\mathbf{u}) = \prod_{d=1}^D \prod_{j=1}^{J_d} p(\mathbf{f}_{d,j}|\mathbf{u}) \prod_{q=1}^Q p(\mathbf{u}_q), \quad (11)$$

where the conditional Gaussian properties allow us to express,

$$p(\mathbf{f}_{d,j}|\mathbf{u}) = \mathcal{N}(\mathbf{f}_{d,j} | \mathbf{A}_{\mathbf{f}_{d,j}\mathbf{u}}, \tilde{\mathbf{Q}}_{\mathbf{f}_{d,j}\mathbf{f}_{d,j}})$$

$$p(\mathbf{u}) = \prod_{q=1}^Q p(\mathbf{u}_q) = \mathcal{N}(\mathbf{u} | \mathbf{0}, \mathbf{K}_{\mathbf{uu}}),$$

with the following definitions,

$$\mathbf{A}_{\mathbf{f}_{d,j}\mathbf{u}} = \mathbf{K}_{\mathbf{f}_{d,j}\mathbf{u}} \mathbf{K}_{\mathbf{uu}}^{-1}, \quad \tilde{\mathbf{Q}}_{\mathbf{f}_{d,j}\mathbf{f}_{d,j}} = \mathbf{K}_{\mathbf{f}_{d,j}\mathbf{f}_{d,j}} - \mathbf{Q}_{\mathbf{f}_{d,j}\mathbf{f}_{d,j}},$$

$$\mathbf{Q}_{\mathbf{f}_{d,j}\mathbf{f}_{d,j}} = \mathbf{K}_{\mathbf{f}_{d,j}\mathbf{u}} \mathbf{K}_{\mathbf{uu}}^{-1} \mathbf{K}_{\mathbf{u}\mathbf{f}_{d,j}}, \quad \mathbf{K}_{\mathbf{f}_{d,j}\mathbf{u}} = \mathbf{K}_{\mathbf{u}\mathbf{f}_{d,j}}^\top.$$

Here the covariance matrix $\mathbf{K}_{\mathbf{f}_{d,j}\mathbf{f}_{d,j}} \in \mathbb{R}^{N \times N}$ is built from the evaluation of all pairs of input data $\mathbf{X} \in \mathbb{R}^{N \times P}$ in the covariance function $\text{cov}[f_{d,j}(\cdot), f_{d,j}(\cdot)] = \sum_{q=1}^Q a_{d,j,q} a_{d,j,q} k_q(\cdot, \cdot)$, the cross covariance matrix $\mathbf{K}_{\mathbf{f}_{d,j}\mathbf{u}} = [\mathbf{K}_{\mathbf{f}_{d,j}\mathbf{u}_1}, \dots, \mathbf{K}_{\mathbf{f}_{d,j}\mathbf{u}_Q}] \in \mathbb{R}^{N \times QM}$ where each block $\mathbf{K}_{\mathbf{f}_{d,j}\mathbf{u}_q} \in \mathbb{R}^{N \times M}$ is formed by the evaluations of $\text{cov}[f_{d,j}(\cdot), u_q(\cdot)] = a_{d,j,q} k_q(\cdot, \cdot)$ between inputs \mathbf{X} and \mathbf{Z}_q , the matrix $\mathbf{K}_{\mathbf{uu}} \in \mathbb{R}^{QM \times QM}$ is a block-diagonal with blocks $\mathbf{K}_{\mathbf{u}_q\mathbf{u}_q} \in \mathbb{R}^{M \times M}$ built from evaluations of $\text{cov}[u_q(\cdot), u_q(\cdot)] = k_q(\cdot, \cdot)$ between all pairs of inducing points \mathbf{Z}_q respectively. Notice that each d -th output of the model can have a different number of inputs, but we have assumed that all outputs associate the same data observations \mathbf{X} to ease the explanation.

4.3 The Evidence Lower Bound

We follow a variational inference derivation similar to the one used for variational inducing kernels for efficient MOGPs (Álvarez et al., 2010) and also in single output GPs (Hensman et al., 2013). This approaches grant us the

application of the HetMOGP model in the context of large data. The goal is to approximate the true posterior $p(\mathbf{f}, \mathbf{u}|\mathbf{y})$ with a variational distribution $q(\mathbf{f}, \mathbf{u})$ by optimising the following ELBO:

$$\mathcal{L} = \mathbb{E}_{q(\mathbf{f}, \mathbf{u})} \left[\log \frac{p(\mathbf{y}|\mathbf{f})p(\mathbf{f}|\mathbf{u})p(\mathbf{u})}{q(\mathbf{f}, \mathbf{u})} \right]. \quad (12)$$

We set a tractable posterior $q(\mathbf{f}, \mathbf{u}) = p(\mathbf{f}|\mathbf{u})q(\mathbf{u})$, where $p(\mathbf{f}|\mathbf{u})$ is already defined in Eq. (11), $q(\mathbf{u}|\mathbf{m}, \mathbf{V}) = \prod_{q=1}^Q q(\mathbf{u}_q)$, and each $q(\mathbf{u}_q) = \mathcal{N}(\mathbf{u}_q|\mathbf{m}_q, \mathbf{V}_q)$ is a Gaussian distribution with mean \mathbf{m}_q and covariance \mathbf{V}_q (Hensman et al., 2015a). To be consistent with the optimisation algorithms introduced in previous sections which focus on minimising an objective function, we write again Eq. (12) as a negative ELBO:

$$\tilde{\mathcal{L}} = \sum_{n=1}^N \sum_{d=1}^D \mathbb{E}_{q_{\mathbf{f}_{d,1}} \dots q_{\mathbf{f}_{d,J_d}}} [g_{d,n}] + \sum_{q=1}^Q \mathbb{D}_{KL}(q(\mathbf{u}_q)||p(\mathbf{u}_q)), \quad (13)$$

where $g_{d,n} = -\log p(y_{d,n}|f_{d,1,n}, \dots, f_{d,J_d,n})$ is the NLL function associated to each output, and the above expectation is computed with regard to the posteriors,

$$q_{\mathbf{f}_{d,j}} := \mathcal{N}(\mathbf{f}_{d,j}|\tilde{\mathbf{m}}_{\mathbf{f}_{d,j}}, \tilde{\mathbf{V}}_{\mathbf{f}_{d,j}}), \quad (14)$$

with the following definitions,

$$\tilde{\mathbf{m}}_{\mathbf{f}_{d,j}} := \mathbf{A}_{\mathbf{f}_{d,j}\mathbf{u}}\mathbf{m} \quad (15)$$

$$\tilde{\mathbf{V}}_{\mathbf{f}_{d,j}} := \mathbf{K}_{\mathbf{f}_{d,j}\mathbf{f}_{d,j}} + \mathbf{A}_{\mathbf{f}_{d,j}\mathbf{u}}(\mathbf{V} - \mathbf{K}_{\mathbf{u}\mathbf{u}})\mathbf{A}_{\mathbf{f}_{d,j}\mathbf{u}}^\top, \quad (16)$$

where mean $\mathbf{m} = [\mathbf{m}_1^\top, \dots, \mathbf{m}_Q^\top]^\top \in \mathbb{R}^{QM \times 1}$ and the covariance matrix $\mathbf{V} \in \mathbb{R}^{QM \times QM}$ is a block-diagonal matrix with blocks given by $\mathbf{V}_q \in \mathbb{R}^{M \times M}$.²

5 Deriving a Fully Natural Gradient Scheme

This section describes how to derive the full natural gradient updates for optimising the HetMOGP. We first detail how to induce an exploratory distribution over the hyper-parameters and inducing points, then we write down the mirror descent algorithm for the model and derive the update equations. Later on, we get into specific details about how to compute the most relevant gradients of the model.

5.1 Specifying an Exploratory Distribution

In this subsection we aim to use the VO perspective as a mechanism to apply an exploratory distribution over the inducing points $\text{vec}(\mathbf{Z}) = \phi(\boldsymbol{\theta}_Z)$, over all the kernel hyper-parameters $\boldsymbol{\alpha}_{\text{all_k}} = \phi(\boldsymbol{\theta}_k)$ with $\boldsymbol{\theta}_k = [\boldsymbol{\theta}_{k_1}^\top, \dots, \boldsymbol{\theta}_{k_Q}^\top]^\top$, and over the vector of linear combination coefficients $\mathbf{w} = \phi(\boldsymbol{\theta}_{\text{LPF}})$ used to generate the LPFs in Eq. (10). The real random vectors $\boldsymbol{\theta}_Z \in \mathbb{R}^{QMP \times 1}$, $\boldsymbol{\theta}_{k_q} \in \mathbb{R}^{H \times 1}$ and $\boldsymbol{\theta}_{\text{LPF}} \in \mathbb{R}^{QJ \times 1}$ are associated to the inducing points, a number of H kernel hyper-parameters per latent function $u_q(\cdot)$, and to the vector \mathbf{w} of linear combination coefficients through a mapping function $\phi(\cdot)$ respectively. We use the quadratic mapping function $\phi(\cdot) = (\cdot)^2$ to guarantee the kernel-hyper parameters to have real positive support $\boldsymbol{\alpha}_{\text{all_k}} = (\boldsymbol{\theta}_k)^2$, and an identity function for both the inducing points $\text{vec}(\mathbf{Z}) = \boldsymbol{\theta}_Z$, and the vector of linear combination coefficients $\mathbf{w} = \boldsymbol{\theta}_{\text{LPF}}$. We use $\boldsymbol{\theta} = [\boldsymbol{\theta}_Z^\top, \boldsymbol{\theta}_k^\top, \boldsymbol{\theta}_{\text{LPF}}^\top]^\top \in \mathbb{R}^{(QMP+QH+QJ) \times 1}$ to refer to all these parameters. Then we specify the exploratory Gaussian distribution $q_\theta := \mathcal{N}(\boldsymbol{\theta}|\boldsymbol{\mu}, \boldsymbol{\Sigma})$ and follow the VO approach in Eq. (3), for this case the objective to bound is not directly the NLL function, but the bound $\tilde{\mathcal{L}}$ already derived in Eq. (13). It is actually a bound to the negative marginal log likelihood. Therefore let us define a new bound as follows:

$$\begin{aligned} \tilde{\mathcal{F}} &= \mathbb{E}_{q_\theta} [\tilde{\mathcal{L}}] + \mathbb{D}_{KL}(q_\theta||p_\theta) \\ &= \mathbb{E}_{q_\theta} \left[\sum_{n=1}^N \sum_{d=1}^D \mathbb{E}_{q_{\mathbf{f}_{d,1}} \dots q_{\mathbf{f}_{d,J_d}}} [g_{d,n}] + \sum_{q=1}^Q \mathbb{D}_{KL}(q_{\mathbf{u}_q}||p_{\mathbf{u}_q}) \right] + \mathbb{D}_{KL}(q_\theta||p_\theta), \end{aligned} \quad (17)$$

where $p_{\mathbf{u}_q} := p(\mathbf{u}_q)$, $q_{\mathbf{u}_q} := q(\mathbf{u}_q)$, and p_θ is a penalisation (or prior) distribution that avoids $\boldsymbol{\Sigma}$ to collapse by forcing additional exploration of $\boldsymbol{\theta}$'s space (Khan et al., 2017b).

²The posterior distribution derives from: $q_{\mathbf{f}_{d,j}} = \int p(\mathbf{f}_{d,j}|\mathbf{u})q(\mathbf{u})d\mathbf{u}$.

5.2 Mirror Descent Algorithm for the HetMOGP

With the purpose of minimising the above objective, we use the mirror descent algorithm in Eq. (9) which additionally exploits the natural-momentum. In the interest of easing the derivation, we use the mean-parameters of distributions $q_{\mathbf{u}_q}$ and $q_{\boldsymbol{\theta}}$ defining $\boldsymbol{\rho}_q = \{\mathbf{m}_q, \mathbf{m}_q \mathbf{m}_q^\top + \mathbf{V}_q\}$ and $\boldsymbol{\eta} = \{\boldsymbol{\mu}, \boldsymbol{\mu} \boldsymbol{\mu}^\top + \boldsymbol{\Sigma}\}$. In this way we can write the mirror-descent algorithm as:

$$\boldsymbol{\eta}_{t+1}, \{\boldsymbol{\rho}_{q,t+1}\}_{q=1}^Q = \arg \min_{\boldsymbol{\eta}, \{\boldsymbol{\rho}_q\}_{q=1}^Q} \langle \boldsymbol{\eta}, \hat{\nabla}_{\boldsymbol{\eta}} \tilde{\mathcal{F}}_t \rangle + \frac{1}{\tilde{\alpha}_t} \mathbb{D}_{KL}(q_{\boldsymbol{\theta}} \| q_{\boldsymbol{\theta}_t}) - \frac{\tilde{\gamma}_t}{\tilde{\alpha}_t} \mathbb{D}_{KL}(q_{\boldsymbol{\theta}} \| q_{\boldsymbol{\theta}_{t-1}}) \quad (18)$$

$$+ \sum_{q=1}^Q \left[\langle \boldsymbol{\rho}_q, \hat{\nabla}_{\boldsymbol{\rho}_q} \tilde{\mathcal{F}}_t \rangle + \frac{1}{\tilde{\beta}_t} \mathbb{D}_{KL}(q_{\mathbf{u}_q} \| q_{\mathbf{u}_{q,t}}) - \frac{\tilde{v}_t}{\tilde{\beta}_t} \mathbb{D}_{KL}(q_{\mathbf{u}_q} \| q_{\mathbf{u}_{q,t-1}}) \right],$$

where $\tilde{\mathcal{F}}_t := \tilde{\mathcal{F}}(\mathbf{m}_t, \mathbf{V}_t, \boldsymbol{\mu}_t, \boldsymbol{\Sigma}_t)$, and $\tilde{\beta}_t$, $\tilde{\alpha}_t$, \tilde{v}_t , and $\tilde{\gamma}_t$ are positive step-size parameters. Now we can solve for (18) by computing derivatives w.r.t $\boldsymbol{\eta}$ and $\boldsymbol{\rho}_q$, and setting to zero. Then we reach the fully natural gradient updates:

$$\boldsymbol{\Sigma}_{t+1}^{-1} = \boldsymbol{\Sigma}_t^{-1} + 2\alpha_t \hat{\nabla}_{\boldsymbol{\Sigma}} \tilde{\mathcal{F}}_t \quad (19)$$

$$\boldsymbol{\mu}_{t+1} = \boldsymbol{\mu}_t - \alpha_t \boldsymbol{\Sigma}_{t+1} \hat{\nabla}_{\boldsymbol{\mu}} \tilde{\mathcal{F}}_t + \gamma_t \boldsymbol{\Sigma}_{t+1} \boldsymbol{\Sigma}_t^{-1} (\boldsymbol{\mu}_t - \boldsymbol{\mu}_{t-1}) \quad (20)$$

$$\mathbf{V}_{q,t+1}^{-1} = \mathbf{V}_{q,t}^{-1} + 2\beta_t \hat{\nabla}_{\mathbf{V}_q} \tilde{\mathcal{F}}_t \quad (21)$$

$$\mathbf{m}_{q,t+1} = \mathbf{m}_{q,t} - \beta_t \mathbf{V}_{q,t+1} \hat{\nabla}_{\mathbf{m}_q} \tilde{\mathcal{F}}_t + v_t \mathbf{V}_{q,t+1} \mathbf{V}_{q,t}^{-1} (\mathbf{m}_{q,t} - \mathbf{m}_{q,t-1}), \quad (22)$$

where $\alpha_t = \tilde{\alpha}_t / (1 - \tilde{\gamma}_t)$, $\beta_t = \tilde{\beta}_t / (1 - \tilde{v}_t)$, $\gamma_t = \tilde{\gamma}_t / (1 - \tilde{\gamma}_t)$ and $v_t = \tilde{v}_t / (1 - \tilde{v}_t)$ are positive step-size parameters.

5.3 Computing the Gradients

The computation of the gradients $\hat{\nabla}_{\boldsymbol{\Sigma}} \tilde{\mathcal{F}}$ and $\hat{\nabla}_{\boldsymbol{\mu}} \tilde{\mathcal{F}}$ is directly influenced by the penalisation (or prior) distribution $p_{\boldsymbol{\theta}}$. For convenience of computing the KL divergence term in Eq. (17), we define a Gaussian distribution $p_{\boldsymbol{\theta}} = \mathcal{N}(\boldsymbol{\theta} | \mathbf{0}, \lambda_1^{-1} \mathbf{I})$ with precision $\lambda_1 > 0$ (Khan et al., 2017b). Therefore, using the Gaussian identities popularized in (Oppen and Archambeau, 2009), we can express the gradients as:

$$\hat{\nabla}_{\boldsymbol{\mu}} \tilde{\mathcal{F}} = \mathbb{E}_{q_{\boldsymbol{\theta}}} [\hat{\nabla}_{\boldsymbol{\theta}} \tilde{\mathcal{L}}] + \lambda_1 \boldsymbol{\mu} \quad (23)$$

$$\hat{\nabla}_{\boldsymbol{\Sigma}} \tilde{\mathcal{F}} = \frac{1}{2} \mathbb{E}_{q_{\boldsymbol{\theta}}} [\hat{\nabla}_{\boldsymbol{\theta}\boldsymbol{\theta}}^2 \tilde{\mathcal{L}}] + \frac{1}{2} \lambda_1 \mathbf{I} - \frac{1}{2} \boldsymbol{\Sigma}^{-1}. \quad (24)$$

Notice that if we assume that $p_{\boldsymbol{\theta}} = q_{\boldsymbol{\theta}}$, then the KL divergence to the right hand side of (17) vanishes (Hensman et al., 2015b; Khan et al., 2017a). Thereby, the above gradients end up with only the first expectation term to the right hand side. This means that, when the optimisation is carried out, the covariance $\boldsymbol{\Sigma}$ collapses rapidly ($\boldsymbol{\Sigma} \rightarrow \mathbf{0}$) without much exploration around the mean $\boldsymbol{\mu}$. The other gradients $\hat{\nabla}_{\mathbf{m}_q} \tilde{\mathcal{F}} = \mathbb{E}_{q_{\boldsymbol{\theta}}} [\hat{\nabla}_{\mathbf{m}_q} \tilde{\mathcal{L}}]$ and $\hat{\nabla}_{\mathbf{V}_q} \tilde{\mathcal{F}} = \mathbb{E}_{q_{\boldsymbol{\theta}}} [\hat{\nabla}_{\mathbf{V}_q} \tilde{\mathcal{L}}]$ depend on the inner gradients $\hat{\nabla}_{\mathbf{m}} \tilde{\mathcal{L}}$ and $\hat{\nabla}_{\mathbf{V}} \tilde{\mathcal{L}}$ of the negative ELBO in Eq. (13). Taking the derivative of $\tilde{\mathcal{L}}$ w.r.t each parameter \mathbf{m}_q and \mathbf{V}_q we arrive to,

$$\hat{\nabla}_{\mathbf{m}_q} \tilde{\mathcal{L}} = \sum_{d=1}^D \sum_{j=1}^{J_d} \mathbf{A}_{\mathbf{f}_{d,j} \mathbf{u}_q}^\top \mathbf{g}_{\mathbf{m}_{d,j}} + \mathbf{K}_{\mathbf{u}_q \mathbf{u}_q}^{-1} \mathbf{m}_q, \quad (25)$$

$$\hat{\nabla}_{\mathbf{V}_q} \tilde{\mathcal{L}} = \sum_{d=1}^D \sum_{j=1}^{J_d} \mathbf{A}_{\mathbf{f}_{d,j} \mathbf{u}_q}^\top \text{diag}(\mathbf{g}_{\mathbf{v}_{d,j}}) \mathbf{A}_{\mathbf{f}_{d,j} \mathbf{u}_q} - \frac{1}{2} [\mathbf{V}_q^{-1} - \mathbf{K}_{\mathbf{u}_q \mathbf{u}_q}^{-1}], \quad (26)$$

where $\mathbf{A}_{\mathbf{f}_{d,j} \mathbf{u}_q} = \mathbf{K}_{\mathbf{f}_{d,j} \mathbf{u}_q} \mathbf{K}_{\mathbf{u}_q \mathbf{u}_q}^{-1}$, the vector $\mathbf{g}_{\mathbf{m}_{d,j}} \in \mathbb{R}^{N \times 1}$ has entries $\mathbb{E}_{q_{f_{d,1,n}, \dots, f_{d,J_d,n}}} [\nabla_{f_{d,j,1}} g_{d,n}]$, the vector $\mathbf{g}_{\mathbf{v}_{d,j}} \in \mathbb{R}^{N \times 1}$ has entries $\frac{1}{2} \mathbb{E}_{q_{f_{d,1,n}, \dots, f_{d,J_d,n}}} [\nabla_{f_{d,j,n}}^2 f_{d,j,n} g_{d,n}]$, and $\text{diag}(\mathbf{g}_{\mathbf{v}_{d,j}})$ is a new matrix with the elements of $\mathbf{g}_{\mathbf{v}_{d,j}}$ on its diagonal. Notice that each distribution $q_{f_{d,j,n}}$ represents the n -th marginal of each distribution $q_{\mathbf{f}_{d,j}}$ from Eq. (14). The above equations allow us to use mini-batches at each iteration of the inference process. Then, instead of using all data observations N , we randomly sample a mini-batch $\mathbf{X}_B \in \mathbb{R}^{B \times P}$ and $\mathbf{y}_B \in \mathbb{R}^{B \times D}$ from the dataset $D = \{\mathbf{X}, \mathbf{y}\}$, here B accounts for the mini-batch size. We simply construct: the matrix $\mathbf{A}_{\mathbf{f}_{d,j} \mathbf{u}_q}$ which becomes $\in \mathbb{R}^{B \times M}$, and the vectors $\mathbf{g}_{\mathbf{m}_{d,j}}$ and $\mathbf{g}_{\mathbf{v}_{d,j}}$ which become $\in \mathbb{R}^{B \times 1}$. Then we scale the first term to the right hand side of Eq. (25) and Eq. (26) by a factor of N/B . We refer to $D_B = \{\mathbf{X}_B, \mathbf{y}_B\}$ as the mini-batch data collection.

5.4 Implementation

In order to implement the proposed method, we have to take into account that our computational complexity depends on inverting the covariance matrix Σ in Eq. (19) and Eq. (24). Such complexity can be expressed as $\mathcal{O}((QMP + HQ + QJ)^3)$, where the factor QMP associated to the number of latent functions, inducing points and input dimensionality tends to dominate the complexity. Likewise, the gradient in Eq. (24) involves the calculation of the Hessian $\hat{\nabla}_{\theta\theta}^2 \tilde{\mathcal{L}}$ which can be computationally expensive and be prone to suffer from non-positive definiteness. To alleviate those complexity issues we assume that $\Sigma = \text{diag}(\sigma^2)$, where $\sigma \in \mathbb{R}^{(QMP+QH+QJ) \times 1}$ is a vector of standard deviations, and $\text{diag}(\sigma^2)$ represents a matrix with the elements of σ^2 on its diagonal. Additionally, we estimate the Hessian in Eq. (24) by means of the Gauss-Newton (GN) approximation $\hat{\nabla}_{\theta\theta}^2 \tilde{\mathcal{L}} \approx (\hat{\nabla}_{\theta} \tilde{\mathcal{L}})^2$ (Bertsekas, 1999)(Khan et al., 2017b). The authors in (Khan et al., 2018) term this approximation as the variational RMSprop method with momentum, they alternatively express Eq. (19) and Eq. (20) as follows,

$$\mathbf{p}_{t+1} = (1 - \alpha_t) \mathbf{p}_t + \alpha_t \mathbb{E}_{q_{\theta}} [\hat{\nabla}_{\theta} \tilde{\mathcal{L}}^2] \quad (27)$$

$$\boldsymbol{\mu}_{t+1} = \boldsymbol{\mu}_t - \alpha_t \left[\frac{1}{\mathbf{p}_{t+1} + \lambda_1 \mathbf{1}} \right] \circ \left(\mathbb{E}_{q_{\theta}} [\hat{\nabla}_{\theta} \tilde{\mathcal{L}}] + \lambda_1 \mathbf{1} \boldsymbol{\mu}_t \right) + \gamma_t \left[\frac{\mathbf{p}_t + \lambda_1 \mathbf{1}}{\mathbf{p}_{t+1} + \lambda_1 \mathbf{1}} \right] \circ (\boldsymbol{\mu}_t - \boldsymbol{\mu}_{t-1}), \quad (28)$$

where \circ represents an element-wise product and we have made a variable change defining a vector $\mathbf{p}_t := \sigma_t^{-2} - \lambda_1 \mathbf{1}$, with $\mathbf{1}$ as a vector of ones. The GN approximation provides stronger numerical stability by avoiding σ^2 to become negative. Also, using $\text{diag}(\sigma^2)$ we reduce the computational complexity from $\mathcal{O}((QMP + HQ + QJ)^3)$ to $\mathcal{O}(QMP + HQ + QJ)$. Algorithm 1 shows a pseudo-code implementation of the proposed method. In practice, we found useful for improving the method’s convergence to update the parameters $\boldsymbol{\mu}_{t+1}$ in Eq. (28) using $\sqrt{\mathbf{p}_t}$ and $\sqrt{\mathbf{p}_{t+1}}$ instead of \mathbf{p}_t and \mathbf{p}_{t+1} .

Algorithm 1 Fully Natural Gradient Algorithm

Input: $\alpha_t, \beta_t, \gamma_t, \nu_t, \lambda_1$

Output: $\Sigma_{t+1}, \boldsymbol{\mu}_{t+1}, \mathbf{V}_{q,t+1}, \mathbf{m}_{q,t+1}$

- 1: set $t = 1$
 - LOOP Process*
 - 2: **while** Not Converged **do**
 - 3: sample $\boldsymbol{\theta}_t \sim q(\boldsymbol{\theta} | \boldsymbol{\mu}_t, \Sigma_t)$
 - 4: randomly sample a mini-batch D_B
 - 5: approx. $\mathbb{E}_{q_{\theta}} [\hat{\nabla}_{\theta} \tilde{\mathcal{L}}]$ and $\mathbb{E}_{q_{\theta}} [\hat{\nabla}_{\theta} \tilde{\mathcal{L}}^2]$ using samples $\boldsymbol{\theta}_t$
 - 6: update \mathbf{p}_{t+1} and $\boldsymbol{\mu}_{t+1}$ using Eq. (27) and (28)
 - 7: compute $\tilde{\nabla}_{\mathbf{m}_q} \tilde{\mathcal{F}}$ and $\tilde{\nabla}_{\mathbf{V}_q} \tilde{\mathcal{F}}$ using Eq. (25) and (26)
 - 8: update each $\mathbf{V}_{q,t+1}$ and $\mathbf{m}_{q,t+1}$ using Eq. (21) and (22)
 - 9: $\Sigma_{t+1} = \text{diag}((\mathbf{p}_{t+1} + \lambda_1 \mathbf{1})^{-1})$
 - 10: $t = t + 1$
 - 11: **end while**
-

6 EXPERIMENTS

In this section we explore the inference performance of the proposed fully natural gradient (FNG) method for optimising all parameters, hyper-parameters and inducing points at the same time. We also test the hybrid (HYB) method proposed by (Salimbeni et al., 2018), and compare the performance against Adam and Stochastic Gradient Descent (SGD) methods. We run experiments on different toy and real datasets, for all the datasets we use a splitting of 75% and 25% for training and testing respectively. The experiments consist on evaluating the method’s performance when starting with 20 different initialisations of the parameters $\boldsymbol{\theta}$ to be optimised. We report the negative evidence lower bound (NELBO) shown in Eq. (13) for the training set and the negative log predictive density (NLPD) error for the test set, this latter metric takes into account the predictions’ uncertainty (Quiñonero-Candela et al., 2006).

6.1 Optimising the HetMOGP on Toy Data

These experiments consist on building three datasets where we can evaluate the inference performance of our method in comparison to the baseline methods. Particularly we are interested in looking at the performance when increasing the number of outputs, which implies rising also the heterogeneity of the output data. Likewise, we are interested in

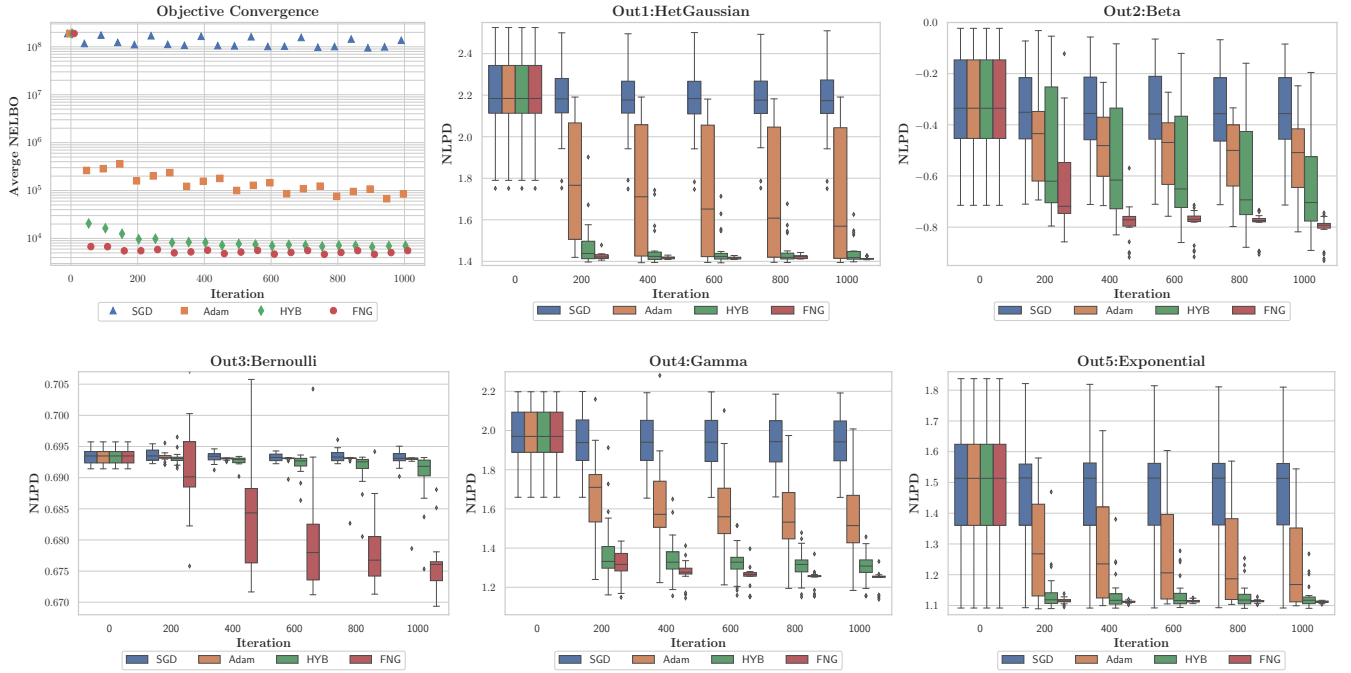


Figure 1: Performance of the different inference methods on the T2 dataset for $P = 10$ using 20 different initialisations. The top left sub-figure shows the average NELBO convergence. The other sub-figures show the box-plot trending of the NLPD over the test set for each output. The box-plots at each iteration follow the legend's order from left to right: SGD, Adam, HYB and FNG. The isolated diamonds that appear in the outputs' graphs represent "outliers".

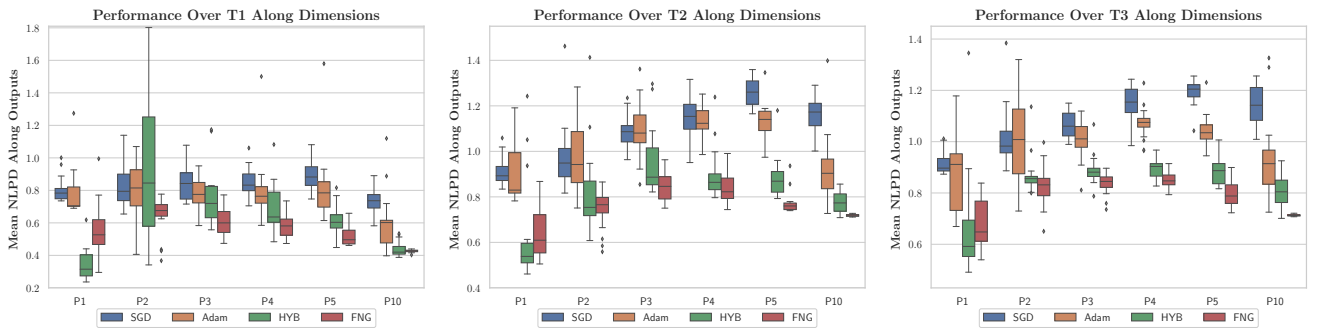


Figure 2: Trending of the Mean NLPD along outputs for 20 different initialisations. Performance over: T1 (left), T2 (middle) and T3. Each sub-figure summarises the Mean NLPD of SGD, Adam, HYB and FNG methods along dimensions $P = \{1, 2, 3, 4, 5, 10\}$. The box-plots at each P follow the legend's order.

assessing the behaviour when increasing the dimensionality of the input space. For all the toys we define an input space $\mathbf{X} \in [0, 1]^{N \times P}$ with $N = 2 \times 10^3$ observations, we analyse a set of different dimensions $P = \{1, 2, 3, 4, 5, 10\}$. We assume a number of $Q = 3$ latent functions $u_q(\cdot) \sim \mathcal{GP}(0, k_q(\cdot, \cdot))$, where we define each $k_q(\cdot, \cdot)$ as an EQ (Exponentiated-Quadratic) kernel, and the set of inducing points per latent function is $\mathbf{Z}_q \in \mathbb{R}^{M \times P}$, with $M = 80$. We run the experiments using mini-batches of 50 samples at each iteration, and we use one sample to approximate the expectations with regard to q_θ in Eq. (17). Below we describe the characteristics of each toy dataset.

Toy Data 1 (T1): the first toy example consists of three outputs $D = 3$; the first output is $y_1 \in \mathbb{R}$, the second $y_2 \in [0, 1]$ and the third $y_3 \in \{0, 1\}$. We use a Heterocedastic-Gaussian (HetGaussian), a Beta and Bernoulli distribution as the likelihoods for each output respectively.

Toy Data 2 (T2): the second toy example consists of five outputs $D = 5$, where the first three are exactly the same ones as T1 with the same likelihoods and the two additional ones are $y_4 \in [0, \infty]$, and $y_5 \in [0, \infty]$. We use a Gamma and Exponential distribution for those latter outputs.

Toy Data 3 (T3): the third toy example consists of ten outputs $D = 10$, where the support of the first five outputs $\{y_d\}_{d=1}^5$ is exactly the same as T2. Also, the last five outputs $\{y_d\}_{d=6}^{10}$ share the same support of the outputs in T2. We use the following ten likelihoods: HetGaussian, Beta, Bernoulli, Gamma, Exponential, Gaussian (with $\sigma_{\text{lik}} = 0.1$), Beta, Bernoulli, Gamma and Exponential. The data of the first five outputs is not the same as the last ones since the distributions of the generative model depend on the linear combination coefficients $a_{d,j,q}$ that generate the LPFs in Eq. (10).³

In order to visualise the convergence performance of the methods we show results for T2 which consists of five outputs, where all of them are used in T3 and three of them in T1. We focus on the example for which $P = 10$ as the dimensionality. Fig.1 shows the behaviour of the different algorithms over T2, where its top left sub-figure shows the average convergence of the objective NELBO after running 20 different initialisations. The figure shows that our FNG method tends to converge faster than the other methods, finding a better local optima solution that minimises the NELBO followed by the HYB, Adam and SGD. The other sub-figures titled from Out1 to Out5 show the model’s average NLPD achieved by each of the methods over the test set. From Fig.1 we can notice that the SGD method does not progress much through the inference process achieving the poorest performance along the diverse outputs. The Adam method presents a big variance along the different outputs, this way showing its ability to explore feasible solutions, but arriving at many different poor local minima. Particularly, for the output 3, a Bernoulli likelihood, the method hardly moves from its initial NLPD value, showing in the figure a tiny variance without much improvement, this means the method lacks of exploration and rapidly becomes trapped in a very poor local minima. The HYB method in general shows smaller error bars than Adam and SGD. Indeed, it reaches low NLPD results for Gamma, HetGaussian and Exponential likelihoods, with similar behaviour to our FNG method in the two latter distributions. Although, it is difficult for HYB to achieve a proper NLPD performance on the distributions Beta and Bernoulli; for the former distribution presents boxes with big variance meaning that it arrives to many different solutions, but the NLPD’s mean shows a trending to weak solutions. For the latter is deficient in exploring, so it also ends up in poor solutions. Our FNG method is consistent along the diverse outputs, usually tending to richer local minima solutions than the other methods. For the Beta and Gamma outputs, FNG makes a confident progress and even shows some “outliers” below its boxes which mean our method has the ability to eventually provide much stronger solutions than the other methods. For the Bernoulli distribution Fig.1 shows that FNG presents big variance boxes, but with a tendency to much better solutions than the other methods. This effect let us confirm that our proposed method actually takes advantage of the stochastic exploration induced over the model hyper-parameters for avoiding weak local minima solutions.

As said before, we aim to evaluate the performance of the inference methods for various numbers of heterogeneous outputs, diverse dimensions, and different initialisations. Therefore, we run experiments over toys T1, T2 and T3 which consist of different number of outputs. For each toy we analyse a set of diverse dimensions $P = \{1, 2, 3, 4, 5, 10\}$, and for each configuration we run 20 trials with different initialisations. For each trial we find the mean NLPD between outputs, then we report the average over all initialisations of that mean NLPD along the outputs. Figure 2 summarises the behaviour along the different dimensions P for each toy. We can notice from the Fig. 2 that our FNG method achieves better test performance along distinct dimensions for all toys, followed by the HYB, Adam and SGD methods. All methods in general tend to present big variances for T1 which consists of three outputs, although this effect is reduced when the number of outputs is increased. This effect is surely related to the support that additional outputs provide to the model for making predictions. Our FNG method in general presents the

³The code with all toy configurations is publicly available in the repository: https://github.com/juanjogg1987/Fully_Natural_Gradient_HetMOGP

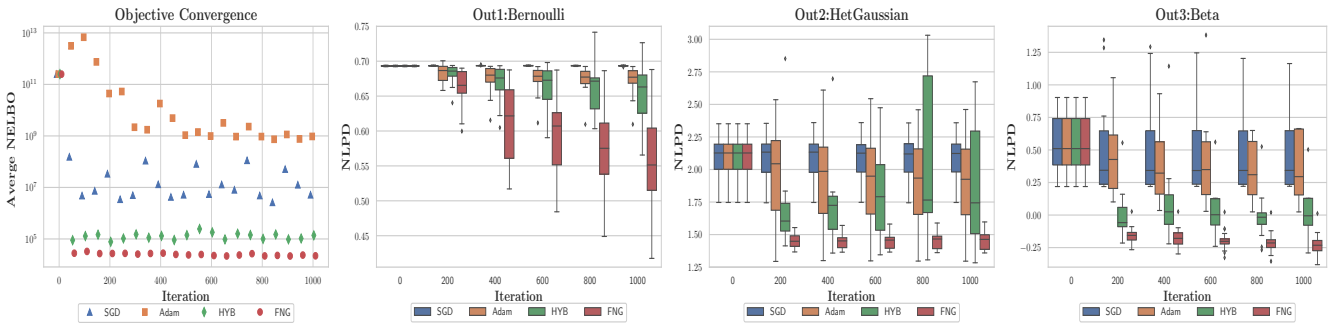


Figure 3: Performance of the diverse inference methods on the HUMAN dataset using 20 different initialisations. The left sub-figure shows the average NELBO convergence of each method. The other sub-figures show the box-plot trending of the NLPD over the test set for each output. The box-plots at each iteration follow the legend’s order from left to right: SGD, Adam, HYB and FNG. The isolated diamonds that appear in the outputs’ graphs represent “outliers”.

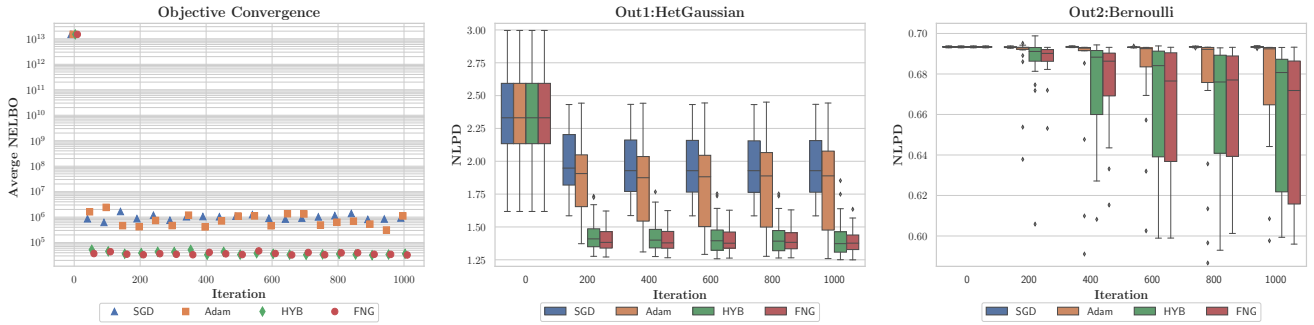


Figure 4: Performance of the diverse inference methods on the LONDON dataset using 20 different initialisations. The left sub-figure shows the average NELBO convergence of each method. The other sub-figures show the box-plot trending of the NLPD over the test set for each output. The box-plots at each iteration follow the legend’s order from left to right: SGD, Adam, HYB and FNG. The isolated diamonds that appear in the outputs’ graphs represent “outliers”.

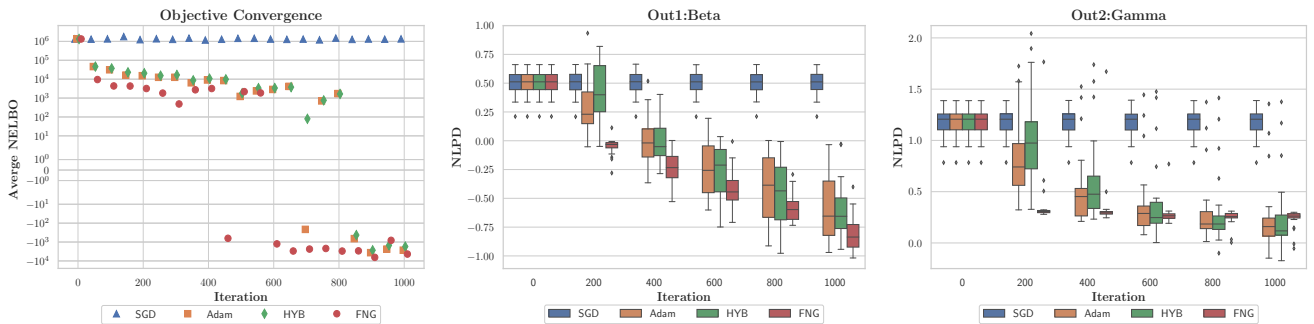


Figure 5: Performance of the diverse inference methods on the NAVAL dataset using 20 different initialisations. The left sub-figure shows the average NELBO convergence of each method. The other sub-figures show the box-plot trending of the NLPD over the test set for each output. The box-plots at each iteration follow the legend’s order from left to right: SGD, Adam, HYB and FNG. The isolated diamonds that appear in the output graphs represents “outliers”.

smallest variance showing its ability to find better local minima solutions even with many outputs. When increasing the dimensionality, the methods tend to degrade their performance, but the less sensitive to such behaviour are the HYB and FNG methods, where the latter, in general achieves the lowest mean NLPD along outputs for the different toy examples. Apart from the heterogeneous toys shown in this paper, we also ran experiments for dimensions higher than $P = 10$, although we noticed that all methods behaved similar except for the SGD which demands a very small step-size parameter that makes it progress slowly. We believe that the toy examples become difficult to control in such dimensions and probably the data observations become broadly scattered. We also explored experiments increasing the mini-batch size at each iteration, we noticed the gradient’s stochasticity is reduced helping to increase the convergence rates of all methods, but the ones using NG perform better. When reducing the mini-batch size, FNG method usually performs better than the others probably due to the fact that additionally exploits the probability structure imposed over the θ hyper-parameters.

6.2 Optimising the HetMOGP on Real Data

For this sub-section we explore the method’s behaviour when using real data. For all experiments the number of inducing points \mathbf{Z}_q per latent function is $M = 80$, and for each latent function $u_q(\cdot)$ we define $k_q(\cdot, \cdot)$ as an EQ kernel. We run the experiments using mini-batches of 50 samples at each iteration, and we use one sample to approximate the expectations with regard to q_θ in Eq. (17). We describe below the three datasets used for the experiments.

Human Dataset: the human behaviour dataset (HUMAN, $N_1, N_2 = 5 \times 10^3, N_3 = 21 \times 10^3, P = 1$) contains information for monitoring psychiatric patients.⁴ It consists of three outputs; the first monitors use/non-use of *Whatsapp* smartphone application, this output has support $y_1 \in \{0, 1\}$, the second represents distance from the patient’s home location, it has support $y_2 \in \mathbb{R}$, and the third accounts for the number of smartphone active *apps*, we rescale it to have support $y_3 \in [0, 1]$. We use a Bernoulli, HetGaussian and Beta distribution as the likelihood for each output respectively. We assume a number of $Q = 5$ latent functions.

London Dataset: the London dataset (LONDON, $N_1, N_2 = 20 \times 10^3, P = 2$) is a register of properties sold in the Greater London County in 2017, consists of two outputs; the first represents house prices with support $y_1 \in \mathbb{R}$ and the second accounts for the type of house, we use two types (flat/non-flat) with $y_2 \in \{0, 1\}$, we use a HetGaussian and Bernoulli distribution as the likelihood for each output respectively. We assume a number of $Q = 3$ latent functions.⁵

Naval Dataset: the naval dataset (NAVAL, $N_1, N_2 = 11 \times 10^3, P = 15$) contains information of condition based maintenance of naval propulsion plants, consists of two outputs; plant’s compressor decay state coefficient and turbine decay state coefficient. We re-scaled both as $y_1, y_2 \in [0, 1]$, and used a Beta and Gamma distribution as the likelihood for each output respectively. We assume a number of $Q = 4$ functions.⁶

Figures 3, 4 and 5 show the NELBO convergence over the training set, together with the average NLPD performance over the test set for HUMAN, LONDON and NAVAL data respectively. With regard to the rate convergence of NELBO for HUMAN and LONDON datasets all methods converge similarly. Nonetheless, for the NAVAL dataset, our FNG approach is the fastest to converge, followed by HYB and Adam; SGD remains without much progress along the iterations.

For the HUMAN dataset, the SGD arrives at a better minimum than Adam, but the Adam’s averaged NLPD is higher across outputs. HYB reaches consistent solutions being better than Adam and SGD, not only in the training process but also in testing along the HetGaussian and Beta outputs. Though, the Bernoulli output limits the overall performance of the method since there is not much improvement along the iterations. Our FNG method also shows a steady performance along outputs, commonly arriving to solutions with lower NLPD than the other methods. Our method presents the biggest variance for the Bernoulli output, implying strong exploration of the solutions’ space for such likelihood that allows it to reach the lowest average NLPD.

For the LONDON dataset Adam converges to a richer minimum of the NELBO than SGD, moreover the NLPD for Adam is, on average, better than the SGD for both HetGaussian and Bernoulli outputs. Particularly, Adam presents for the Bernoulli output few “outliers” under its boxes that suggest it can find sporadically rich local optima, but its general trend was to provide poor solutions for that specific output in contrast to the HetGaussian output. The HYB and FNG arrive to a very similar value of the NELBO, both being better than Adam and SGD. HYB and FNG methods attain akin NLPD metrics for the HetGaussian output, though our method shows smaller boxes being

⁴The HUMAN dataset is captured using the smartphone *app* EB2, For more information visit <https://www.eb2.tech/>.

⁵See <https://www.gov.uk/government/collections/price-paid-data> for information about LONDON dataset.

⁶See <http://archive.ics.uci.edu/ml/datasets> for the NAVAL data information.

more confident along iterations. Both methods present big variances for the Bernoulli output, but the average and median trend of our approach is much better, being more robust to initialisation than HYB method.

The NLPD performance for the NAVAL dataset shows in Fig. 5 that SGD method cannot make progress, we tried to set a bigger step-size, but usually increasing it derived numerical problems due to ill-conditioning. The methods Adam and HYB show almost the same behaviour along the NELBO optimisation, in fact the NLPD boxes for the Beta and Gamma outputs look quite similar for both methods. The difference of performance can be noticed for the Beta output, where at the end, HYB method becomes more confident reducing its variance. Our FNG method ends up with a slightly upper NLPD solution in the Gamma output in comparison to Adam and HYB, but being more confident showing a smaller spread in the boxplot across iterations. For the Gamma output, FNG shows at the end some "outliers" under the NLPD boxes, accounting for sporadic convergence to strong solutions. For the Beta distribution, our method arrives to a lower solution with the finest NLPD in comparison to SGD, HYB and Adam.

7 Discussion and Conclusion

In practice we noticed that some likelihoods (e.g. HetGaussian, Gamma) tend to strongly influence the value of the objective function (NELBO), so the optimisers HYB, Adam and SGD are prone to find solutions that focus on such sort of likelihoods, while neglecting the others with less influence, for instance a Bernoulli or Beta as shown in Fig.1. Although, our proposed scheme presents a more consistent performance achieving rich solutions across the different sort of outputs' distributions. Also, we noticed that our method is the least sensible to reduce its performance when increasing the dimensionality. Apart from the experiments shown above, we also tested the behaviour of the methods when all the outputs share the same likelihoods; in general we realised that Adam, HYB and FNG provide similar solutions, but our method tends to converge faster, followed by the HYB and Adam methods. When using the SGD method we had to set a very small step-size parameter, because using big step-sizes makes the model to easily become ill-conditioned.

In this paper we have shown how a fully natural gradient scheme improves optimisation of the HetMOGP model reaching better local optima solutions with higher test performance rates than HYB, Adam and SGD methods. We have shown that our FNG scheme provides rich local optima solutions, even when increasing the number of outputs and dimensions. We think our method can also be an alternative tool for improving optimisation over a single output GP model. In fact, as a future work we could explore the behaviour of the proposed scheme over other type of GP models, for instance Deep GPs. Likewise, it would be challenging to explore a scalable way to implement the method using a full covariance matrix Σ which can exploit more correlations between all hyper-parameters.

Acknowledgment

The authors would like to thank Emtiyaz Khan for all the feedback related to mathematical aspects of the method. JJG is being funded by a scholarship from the Department of Computer Science, University of Sheffield. MAA has been financed by the EPSRC Research Projects EP/R034303/1 and EP/T00343X/1.

References

- Mauricio A. Álvarez, D. Luengo, M. K. Titsias, and Neil D. Lawrence. Efficient multioutput Gaussian processes through variational inducing kernels. In *AISTATS*. 2010.
- Mauricio A. Álvarez, Lorenzo Rosasco, and Neil D. Lawrence. Kernels for vector-valued functions: A review. *Found. Trends Mach. Learn.*, 4(3):195–266, March 2012. ISSN 1935-8237.
- Mauricio Alexander Álvarez and Neil D. Lawrence. Sparse convolved Gaussian processes for multi-output regression. In *NIPS*, pages 57–64. 2009.
- Shunichi Amari. Natural gradient works efficiently in learning. *Neural Computation*, 10(2):251–276, February 1998.
- D.P. Bertsekas. *Nonlinear Programming*. Athena Scientific, 1999.
- Christopher M. Bishop. *Pattern Recognition and Machine Learning*. Springer-Verlag New York, Inc., 2006.
- David M. Blei, Alp Kucukelbir, and Jon D. McAuliffe. Variational inference: A review for statisticians. *Journal of the American Statistical Association*, 112(518):859–877, 2017.

- E.K.P. Chong and S.H. Zak. *An Introduction to Optimization*. Wiley Series in Discrete Mathematics and Optimization. Wiley, 2013. ISBN 9781118515150.
- James Hensman, Nicolás Fusi, and Neil D. Lawrence. Gaussian processes for big data. In *UAI*, 2013.
- James Hensman, Alexander G. de G. Matthews, and Zoubin Ghahramani. Scalable variational Gaussian process classification. In *AISTATS*, 2015a.
- James Hensman, Alexander G. de G. Matthews, Maurizio Filippone, and Zoubin Ghahramani. MCMC for variationally sparse Gaussian processes. In *NIPS*, pages 1648–1656. MIT Press, 2015b.
- Dave Higdon. Space and space-time modeling using process convolutions. pages 37–56. Springer London, 2002.
- A. G. Journel and C. J. Huijbregts. *Mining Geostatistics*. Academic Press, London, 1978.
- Mohammad E Khan, Pierre Baque, François Fleuret, and Pascal Fua. Kullback-Leibler proximal variational inference. In *NIPS*, pages 3402–3410. 2015.
- Mohammad Emtiyaz Khan and Wu Lin. Conjugate-computation variational inference: Converting variational inference in non-conjugate models to inferences in conjugate models. In *AISTATS*, 2017.
- Mohammad Emtiyaz Khan, Wu Lin, Voot Tangkaratt, Zuozhu Liu, and Didrik Nielsen. Variational adaptive-Newton method for explorative learning. *CoRR*, abs/1711.05560, 2017a.
- Mohammad Emtiyaz Khan, Zuozhu Liu, Voot Tangkaratt, and Yarin Gal. Vprop: Variational inference using RMSprop. *CoRR*, abs/1712.01038, 2017b.
- Mohammad Emtiyaz Khan, Didrik Nielsen, Voot Tangkaratt, Wu Lin, Yarin Gal, and Akash Srivastava. Fast and scalable Bayesian deep learning by weight-perturbation in adam. In *ICML*, pages 2616–2625, 2018.
- Pablo Moreno-Muñoz, Antonio Artés-Rodríguez, and Mauricio A. Álvarez. Heterogeneous multi-output Gaussian process prediction. In *NeurIPS*, pages 6712–6721, 2018.
- Kevin P. Murphy. *Machine Learning: A Probabilistic Perspective*. MIT Press, 2013.
- Manfred Opper and Cédric Archambeau. The variational Gaussian approximation revisited. *Neural Comput.*, 21(3):786–792, March 2009. ISSN 0899-7667.
- Joaquin Quiñero-Candela and Carl Edward Rasmussen. A unifying view of sparse approximate Gaussian process regression. *JMLR*, 6:1939–1959, 2005.
- Joaquin Quiñero-Candela, Carl Edward Rasmussen, Fabian Sinz, Olivier Bousquet, and Bernhard Schölkopf. Evaluating predictive uncertainty challenge. pages 1–27. Springer Berlin Heidelberg, 2006.
- Garvesh Raskutti and Sayan Mukherjee. The information geometry of mirror descent. *IEEE Trans. Information Theory*, 61(3):1451–1457, 2015.
- Carl Edward Rasmussen. *Gaussian processes for machine learning*. MIT Press, 2006.
- Hugh Salimbeni, Stefanos Eleftheriadis, and James Hensman. Natural gradients in practice: Non-conjugate variational inference in Gaussian process models. In *AISTATS*, pages 689–697, 2018.
- Hugh Salimbeni, Vincent Dutordoir, James Hensman, and Marc Deisenroth. Deep Gaussian processes with importance-weighted variational inference. In *ICML*, pages 5589–5598, 2019.
- Alan Saul, James Hensman, Aki Vehtai, and Neil D Lawrence. Chained Gaussian processes. *AISTATS*, 2016.
- Edward Snelson and Zoubin Ghahramani. Sparse Gaussian processes using pseudo-inputs. In *NIPS*, pages 1257–1264. 2006.
- Joe Staines and David Barber. Optimization by variational bounding. In *ESANN*, 2013.
- Michalis K. Titsias. Variational learning of inducing variables in sparse Gaussian processes. In *AISTATS*, 2009.
- Mark van der Wilk. Sparse Gaussian Process Approximations and Applications. *PhD Thesis, University of Cambridge*, 2018.
- Daan Wierstra, Tom Schaul, Tobias Glasmachers, Yi Sun, Jan Peters, and Jürgen Schmidhuber. Natural evolution strategies. *J. Mach. Learn. Res.*, 15(1):949–980, January 2014. ISSN 1532-4435.